The Successful Incorporation of Nd Into Ba Site of $Y_{0.9}Ho_{0.1}Ba_{2-y}Nd_yCu_3O_{7-\delta}$ Bulk Superconductors

N. K. Saritekin[1,*] and A. T. Üzümcü[2]

[1]*Physikalisches Institut, Center for Quantum Science (CQ) and LISA+, Universität Tübingen, Auf der Morgenstelle 14, D-72076 Tübingen, Germany*

[2]*Institute of Chemical Technology and Polymer Chemistry, Karlsruhe Institute of Technology (KIT), Engesserstraße 18, 76131 Karlsruhe, Germany*

Abstract: This inclusive study reports the effect of the Nd atoms on the mechanical, microstructural, electrical and superconducting characteristics of $Y_{0.9}Ho_{0.1}Ba_{2-y}Nd_yCu_3O_{7-\delta}$ superconductors with the aid of standard characterization methods, including X-ray diffraction, scanning electron microscopy, the bulk density, dc resistivity, and transport critical current density. The experimental results such as the degree of granularity, hole localization effect, room temperature resistivity, critical transition temperature, degree of the broadening, thermodynamic fluctuations, crystallinity, crystal plane alignments, crystal structure, grain size, phase purity and lattice parameters, the appearance of flux pinning centers, grain boundary weak-links, surface morphologies elemental compositions and distributions belonging to Y-site Ho and Ba-site Nd substituted Y-123 superconducting samples are discussed in detail for the first time. All the experimental findings show that the microstructural, electrical, mechanical and superconducting properties regularly improve with the increment in the HcN (Ho constant+Nd changeble) until a certain value of y=0.100, beyond which the characteristics tend to retrograde rapidly. This is attributed to the fact that excess penetration of the Nd damages the crucial properties given above.

Keywords: X-ray diffraction, Electron microscopy, Ceramics, Mechanical characterization, Grain boundaries.

1. INTRODUCTION

Although lanthanides such as trivalent La, Ce, Eu, Gd, Pr were wanted to be added to Ba, they could be added to Y. In addition, there is no significant change in unit cell parameters when Lu and Sc are substituted for Ba. While there were different variations in the unit cell parameters *a* and *b* when La was added to the Ba region, a large reduction in *c* occurred, and the orthorhombicity and critical temperatures decreased overall. At the same time, oxygen content and normal state resistivity in the prepared samples increased with La content. The material has turned into a metal-semiconductor. There is a correlation between T_c and the deformation of the unit cell [1, 2].

Divalent elements such as M = Mg, Ca, and Sr caused a decrease in superconductivity properties in the $Y(Ba_{1-x}M_x)_2Cu_3O_\delta$ system. In solid solutions, T_c decreases with the size M. Mg was found to be substituted in the Cu region [3].

Substitution of Hg in solid solutions was used to prepare a 90 K superconductor in air, $Y(Ba_{1-x}Hg_x)_2Cu_3O_\delta$. HgO separates the sample by oxidation, and Hg is lost by volatilization [4].

The addition of monovalent elements to Ba has been studied. For solid solutions $Y(Ba_{1-x}A_x)_2Cu_3O_\delta$ A=Li, Na, K, Rb, and Cs, the unit cells remain orthorhombic and constant, and the critical temperatures decrease slightly [1, 5].

The effect of oxygen is very high on the electronic properties of high-temperature superconductors. Normally, an oxygen atom gains two electrons from another atom. If there is a lack of oxygen, there will be two free electrons that can go anywhere in the crystal. Oxygen vacancies change the number of free carriers in the crystal lattice. According to the charge transmission model, oxygen deficit occurs in CuO chains. As a result, $CuO_{1-\delta}$ structures are formed, while the CuO_2 layers remain chemically unchanged. In YBCO doping, the amount of oxygen should be controlled. Because the amount of oxygen affects the number of carriers in the CuO_2 plane and determines the T_c value [6-9].

Changes in the crystal structure of YBCO with different substitutions were investigated by electron microscopy and correlated with physical properties. From these substitute materials. Oxygen sequencing was investigated in R = Er, Nd, Sm, Pr Y, and Yb and superconducting $RBa_2Cu_3O_{7-\delta}$ ceramic materials. The critical temperature T_c was obtained as a function of the oxygen deficiency of the compound. Small Fe substitutions for Cu have a lively effect on T_c and

*Address correspondence to this author at Physikalisches Institut, Center for Quantum Science (CQ) and LISA+, Universität Tübingen, Auf der Morgenstelle 14, D-72076 Tübingen, Germany; Tel: +49 7071 29-76324; Fax: +49 7071 29-5406; E-mail: n.kemalsaritekin@gmail.com

microstructure. The twin field size is reduced, and a "tweed" pattern is formed by means of arbitrarily distributed Fe^{+2} ions or Fe^{+2} clusters as fixation centers for twin interfaces. Ga or Co inclusions for Cu change the structure of the "chain" layer [10-13].

The effects of dopants and impurities depend on their valance, ionic radius, substitutional sites, electronic configuration, solubility, nature (magnetic, nonmagnetic, metal, semiconducting, etc.)

2. EXPERIMENTAL DETAILS

The solid-state reaction method is the most common preparation route for ceramic superconductors since researchers have better processing control and do not require special equipment.

Samples of the nominal composition $Y_{0.9}Ho_{0.1}Ba_{2-y}Nd_yCu_3O_{7-\delta}$ have been prepared by the conventional solid-state reaction technique.

Therefore, the chemical equilibrium equation was written as following:

$(0.45)Y_2O_3+(0.05)Ho_2O_3+(2-y)BaCO_3+(0.5y)Nd_2O_3+$

$3CuO+nO_2 \rightarrow Y_{0.9}Ho_{0.1}Ba_{(2-y)}Nd_yCu_3O_{7-\delta} + CO_2$
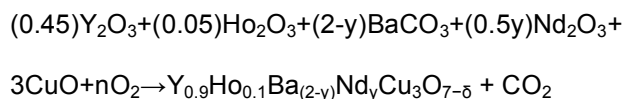
From this formula, the quantities of reactants to produce approximately 6 grams of the unreacted compound were prepared.

The mixed powders were calcined in an alumina crucible in the air at temperatures of 930 °C, for 24 hours in the furnace. Throughout our experiments, the heating and cooling rates of the temperature were chosen to be 3 and 2 °C min-1, respectively.

As well known, the sintering process performed at higher temperatures than the calcinationp process helps the carbons in the starting powders to release. This is very important to save the formation of the impurity phases. The calcined material was reground for two hours in mortar again and pressed into pellets of 40x5x2 mm^3 at 330 MPa with a manual hydraulic press to increase the connection areas of the grains.

The DTA results indicate that Ho and Nd addition can change (decrease) the melting temperature of Y-system superconductors. This may be because the Ho^{+3}, Nd^{+3} and Nd^{+2} ionic radii are different from the Y^{+3} and Ba^{+2} ionic radii. Moreover, the atmosphere has an important influence on melting temperature. This

has the potential for fabricating oxide superconductors with a metal substrate, since the superconductor cannot react with some metals at a lower temperature [14].

The pellets were sintered in air at 945 °C for 24 h and then cooled down to room temperature. The heating and cooling rates of the temperature were chosen to be 3 and 1 °C min^{-1}, respectively. At the same time, O_2 was given between 716 °C and 416 °C while the pellets sintered were cooling.

The annealing and evaporation process were performed in a programmable tube furnace from PROTHERM (Model PZF 12/75/700). The aim of annealing the samples was to complete the phase formation, improve the mechanical properties, obtain better grain growth and enhance the superconducting properties. In forthcoming sections, the superconducting ceramics prepared with Ho constant (x=0.100) different Nd stoichiometry such as 0, 0.025, 0.050, 0.100, 0.250 and 0.500 will be abbreviated as HcN0, HcN1, HcN2, HcN3, HcN4 and HcN5, respectively.

X-Ray diffraction analysis (XRD), resistivity, transport critical current density, bulk density, and scanning electron microscopy (SEM) are performed to determine the effect of Nd on the microstructural, electrical, mechanical and superconducting properties of the superconducting bulks produced.

X-Ray diffractometer was used to examine the structure of a material from the scattering pattern. The working mechanism was subject to the interaction between high-energy beams of radiation or charged particles and a material. X-ray diffraction measurements were exerted with the aid of a Rigaku Multiflex+XRD diffractometer with CuKα target giving a monochromatic beam (wavelength of 1.54 Å) in the range of 2θ=3–60° at a scan speed of 3°/min and step increment of 0.02° in an air atmosphere at the room temperature. The XRD patterns obtained allow us to discuss the change of the texturing, phase purity, crystal structure, grain size (from Scherrer–Warren approach), and cell parameters (accuracy of ±0.01 Å).

The electrical characteristics belonging to the pure and substituted Y-123 superconducting ceramics are studied by means of the temperature dependent-resistivity measurements using 5 mA DC current through the sample surface in the He gas contact cryostat with provision for the vacuum in the

temperature range of 40-110 K. The standard four-probe measurements are exerted with a Keithley 2400 source meter and a Keithley 2700 multimeter. The four-point contacts are made by the silver paint to be rid of the extra resistivity. The current was applied to the two outer electrical contacts. The voltage drop across the two inner electrical contacts was measured against temperature.

Additionally, a temperature value, where the resistance started to decrease sharply, is called the samples' onset critical temperature (T_c^{onset}). In contrast, the offset transition temperature (T_c^{offset}) is defined as the temperature at which R=0 Ω (within the sensitivity of the measurement system).

The measurement of the potential difference between the inner contacts is used to obtain the maximum current passing through a material or critical current density of a material when the current applied to the material is regularly enhanced at the constant temperature at which this material exhibits the superconducting properties and so the potential difference is recorded as zero. However, when the critical value is reached, the potential difference starts to increase immediately due to the presence of the resistance. In this work, the transport critical current experiments are performed in self-field using a four-probe method at the liquid nitrogen temperature of 77 K in zero magnetic fields. A PCE Power Control GEN1500 programmable current source (6V-200A) and a Keithley 2700 Multimeter were used for I-V measurements. The experimental data obtained are recorded by Labview software. The current applied parallel to the direction of the pressed surface is ramped at a constant rate (100 mA/s) for the entire sample. The critical current (I_c) values of the samples are defined with the 1 µV/cm criterion. The J_c values are calculated from the I_c and the total cross-sectional area of the samples studied.

At the same time, the bulk densities of the superconducting samples are experimentally measured via the density measurement kit based on the Archimedes water displacement method. They are shown in Table **2**.

A high-energy focused beam of electrons scans the surface of a material in the Scanning Electron Microscope (SEM). After the interaction between the incident electrons and atoms in the material, a signal containing the information about the surface topography of the material appears. Micrographs of the samples were magnified approximately 3000 and 5000 times, and a magnification bar was given on each micrograph. In this study, the microstructural (surface morphology, crystallinity, crystal plane alignments, porosity, melting, microvoids, cracks, grain size distribution, and connectivity between the superconducting grains) analyses are performed by a Jeol scanning electron microscope (Model Number: JEOL 6390-LV) at the operating voltage of 20 kV with a resolution power of ≈3 nm.

3. RESULTS AND DISCUSSIONS

3.1. XRD Analyses

In this comprehensive study, X-ray diffraction (XRD) patterns of Ba-site Nd-substituted compounds recorded at room temperature allow us to determine crystal plane alignment, phase purity, crystal structure, crystallite size, and lattice parameters. The XRD patterns obtained for the samples between 20° and 60° are given in Figure **1**. It can be seen from the diagrams in this figure that the corresponding Miller indices *h k l* are attributed to the perovskite-based Y-123 phase, with other characteristic peaks marked on the patterns corresponding to the $BaCuO_2$, $Y_2Ba_4Cu_7O_{14+x}$ (Y-247), and $YBa_2Cu_4O_8$ (Y-124) phases. In particular, it is natural to say that Y-124 and Y-247 can easily act as an intergrowth within the perovskite-based Y-123 phase as a result of the additional Cu-O chain layer adjacent to the Ba-O plane resulting in the double chain in the structure [15].

While the superconductivity of the HcN superconducting matrix is improved by increasing the Nd doping level in the Ba region up to y=0.100 at a constant value of x=0.100, it deteriorates at y=0.250 and turns into a tetragonal structure at y=0.500. In fact, the HcN5 compounds present an almost tetragonal structure due to the mixture phases and the occupation of specifically unfilled O5 sites in CuO_x chains in the system. That is, (x=0.100) Ho inclusions and excess (y>0.250) Nd inclusions are unfavorable for the formation of the Y-123 phase.

It should be underlined here that the absence of any different phases containing the Ho and Nd impurities and other cation does not show a solubility limit of Ho and Nd in the Y-123 system up to the content level of x=0.100 and y=0.250, respectively. Namely, the solid solubility of the Y-site Ho and Ba-site Nd substituted compounds are found to be greater than x=0.100 and y=0.250, respectively [16]. The reason for this is that
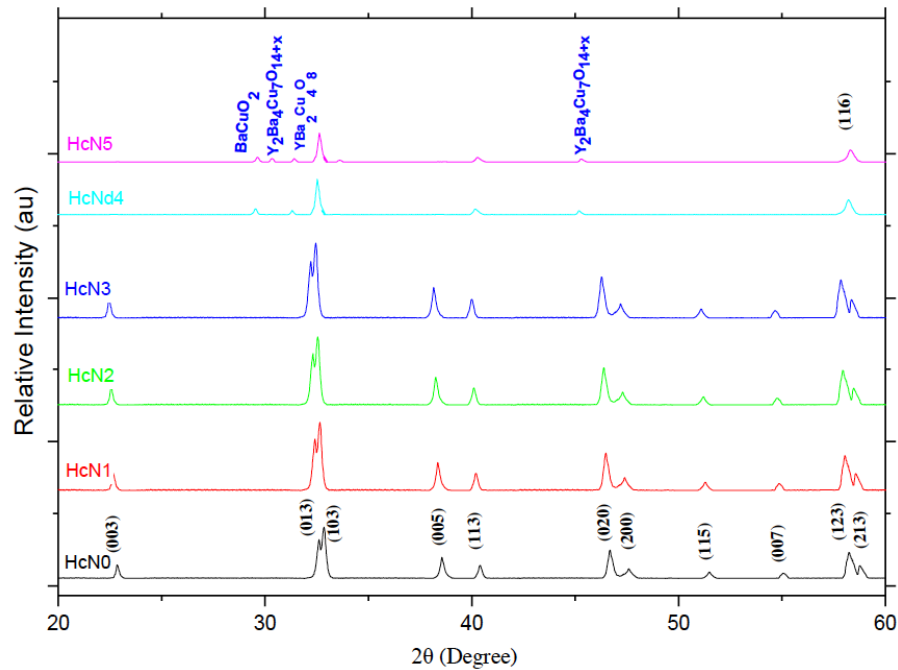
Figure 1: XRD patterns of compounds of Ho constant (x=0.100) and Nd variables (y=0 to y=0.500).

the Ho^{+3} inclusions are added to the Y-123 crystal structure by changing the Y^{+3} individuals up to a certain x=0.100 dopant content level, and the same feature is observed between Ba^{+2} and Nd^{+2} until y=0.250 [17, 18]. At the same time, the figures ensure that each sample mentioned in this study exhibits a polycrystalline superconducting phase, in which diffraction lines are more intense as Nd concentration levels increase up to y=100 in the Y-123 superconducting system. It is noteworthy here that the increased grain growth and much greater peak density indicating grain orientation results in an increase in the critical current density [19].

From the Ho constant (x=0.100) and Nd variable content level of y=0.100, the peaks belonging to the Y-123 phase begin to decrease rapidly [20]. In the case of the HcN4 compound, some peaks such as 003, 013, 005, 113, 020, 200, 115, 007,123, and 213 disappear immediately while the 116 peaks of the characteristic tetragonal crystal structure appear instantaneously. It is even well known from the literature that in the orthorhombic crystal structure, the split diffraction peaks are high-intensity and low-angle around 47.6° (020 and 200) and 58.3° (123 and 213) at 2teta [21]. Regarding the tetragonal crystal structure, the split peaks given above start to coalesce with each other at low-intensity and high-angle (reversion of values in the angle and intensity). The long and short of it is that the crystal plane alignments (known as texturing) and crystallinity of the poly-crystallized Y-123 bulk samples

are disorganized by the excessive Nd impurities. Likewise, the HcN4 and HcN5 samples exhibit the different phase formations with respect to $BaCuO_2$, $Y_2Ba_4Cu_7O_{14+x}$ (Y247), and $YBa_2Cu_4O_8$ (Y124) due to the additional Cu–O chains layer adjacent to the Ba–O planes resulting in the double chain layers in the Y-123 system [15].

Moreover, the variation of the cell parameters *a*, *b,* and *c* in the superconducting matrix with the Nd doped component (leading to shifting of the peaks) allows us to examine the change in superconducting properties of the oxygen-deficient Y-123 system. Whether the crystal structure of the system is orthorhombic or tetragonal can be determined by the *a* and *b* axis lengths. As is well known, the variation of oxygen content in the Cu–O chains [Cu1 region] and the Cu–O_2 planes [Cu2 region] causes an orthorhombic-tetragonal (O-T) transition due to the reorganization of the unit cell structure. That is, the layers (BaO/CuO_2/Y/CuO_2/BaO) in Y-123 superconducting material are interconnected by a layer of Cu and O atoms with variable composition Cu–O_x. The oxygen atoms present in the YBCO are considered O1, O2, O3, O4 and O5. Among them, O1 and O5 sites are located in Cu-O_x strings (Cu–O chains), and O2 and O3 sites exist in the basal copper (Cu–O_2) planes. As the last Oxygen atom, the O4 atom lies in the Ba–O plane [22]. It should be underlined that the rare earth (RE) layer coexists with those deprived of oxygen.

Also, the fully filled O1 (affecting the lattice parameter *b*) and empty O5 (related to the lattice parameter a) allow us to determine why the *b*-axis length is longer than the *a*-axis length for the orthorhombic crystal structure (inherited traits) [23]. It means that the oxygen changes in the Cu–O chains disrupt the crystal structure (structural phase transition from orthorhombic to pseudotetragonal) as a result of the change in the *a* and *b* axis lengths owing to the external forces such as annealing ambient, composition, heat-treatment, type, purity and amount of the chemicals. The first corresponds to the O2 site while the second is attributed to the O3 site located in the Cu–O_2 plane. This study determined the lattice lengths in the orthorhombic unit cell structure using the least-squares technique.

$$d = \frac{1}{\sqrt{\left(\frac{h}{a}\right)^2 + \left(\frac{k}{b}\right)^2 + \left(\frac{l}{c}\right)^2}} \tag{1}$$

According to the calculated results in Table **1**, initially the a and b axis lengths continuously decrease from 3.820 Å to 3.781 Å and from 3.887 Å to 3.870 Å for the HcN compound, respectively, due to the rise in the hybridization of the in-plane Cu(3d) and O(2p) orbitals (Cu–O2 plane) [24, 25] while the c-axis length extends from 11,726 Å to 11,797 Å with the increase in the Ho constant (x=0.100), Nd variable contribution level up to y=0.100 after which the cell parameters *b* and specially *a* begin to enlarge rapidly owing to the enhacement of the electrons into anti-bonding orbital [26]. In contrast, the lattice parameter *c* tends to shrink significantly, and the value *c* actualy reaches a local minimum for the concentration value of y=0.250 for the HcN sample. The decrease in the *c*-axis length is due to preferentially substituting Ho and Nd inclusions in the Cu1 region of the system. In other words, the excessive Nd substitution at the Ba site disrupts the major (Y-123) phase as a result of the hole filling (localization). Besides, this behavior (firstly increase then decrease in *c* value) can be explained by the fact that the ionic radius of Nd^{2+} (143 pm) is slightly smaller compared to Ba^{2+} (149 pm), leading to regular expansion of the cell parameter *c* with the rise of the Nd concentration in the Y-123 up to the certain content value of x=0.100 and y=0.100 beyond which the *c* axis length begins to shrink quickly. This is consistent with the fact that the Ho^{3+} and Nd^{2+} ions can be substituted for the Cu^{2+} individuals in the crystal structure after the critical value of x=0.100 and y=0.100, supported by the findings of the EDS measurement [27]. In other words,

hole filling plays a dominant role in determining the superconductivity of Ho and Nd substituted Y-123s.

In addition, whether Ba/Nd substitution has been performed successfully or not can be checked with the following equation, by which we can calculate the oxygen concentrations in the unit cells of the samples mentioned in this study [28]:

$$y = 7 - \frac{c - 11.68}{0.1501} \tag{2}$$

The calculated oxygen concentrations are provided in Table **1**. It can be seen from the table that the values ranged from 6,8 (for the virgin sample) to 8,822 (for the HcN4 compound). It should be noted here that the value initially dropped to a local minimum of 6,684 (for the HcN3 sample) and then increased significantly to 8,822 owing to the significant decrease in the cell parameter *c*, confirming that the Nd nanoparticles mainly occupied around the Cu1 sites in the crystal structure [21].

Additionally, the X-ray diffraction patterns allow us to examine how the crystallite (grain) size changes with Nd foreign atoms in the Y-123 superconducting samples. In this context, we calculate the grain size of the compounds by Scherrer–Warren equation for the 5 highest intensities of diffraction lines [29].

$$t = \frac{0.941\lambda}{B\cos\theta_B} \tag{3}$$

where t represents the thickness of the crystallite dimension, λ relates to the wavelength of the XRD source, ϴB denotes the Bragg angle, and B (in radian unit) shows the full width at half maximum (FWHM) of the Bragg peak. The results obtained are listed in Table **1**. According to the table, the materials take larger and larger crystallite sizes (from 80 nm to 93 nm) with the increase of the Nd particles in the HcN superconducting matrix up to y=0.100 after which the value tends to decrease towards the local minimum size value of 47 nm and the materials have smaller and smaller crystallite sizes with the enhancement of the Nd particles in the superconducting HcN from x=0.100 to y=0.250 with worst crystallinity and connectivity between grains. This change in the average crystallite size approves why both the superconducting characteristics worsen rapidly and phase transits from orthorhombic to pseudotetragonal structure with the excess only Nd nanoparticles inserted in the HcN superconducting sample. The SEM images even supports this finding.

Table 1: Experimental XRD Results for every Superconducting Sample of HcN

Samples	HcN Content	Lattice Parameters			d(c)	Grain Size	F Values
	y	a (Å)	b (Å)	c (Å)		(nm)	
HcN0	0.000	3.820	3.887	11.726	6.758	80	0.251
HcN1	0.025	3.819	3.879	11.735	6.723	84	0.261
HcN2	0.050	3.813	3.878	11.745	6.698	87	0.273
HcN3	0.100	3.781	3.870	11.797	6.684	93	0.289
HcN4	0.250	3.835	3.895	11.406	8.822	47	0.161
HcN5	0.500	…	…	…	…	…	…

Finally, using the XRD data, we calculate the Lotgering index (F) of the mentioned materials with the following formula to measure the degree of c-axis orientation in the crystal structure [30]. A measure of texture or grain orientation known as F values of the samples are written in Table **1**. As the content of Nd increase up y=0.100, F increases. That is, the orientation or texturing of HcN grains increases monotonicaly upto y=0.100.

It is clear from the table that the crystal plane alignments (texturing of the Y-123 superconducting grains) improve monotonously with increasing the Nd inclusions in the system up to y=0.100, and beyond that, they are severely disturbed by the interference of the excess Ho particles into the HcN matrix.

$$F_{(123)} = \frac{\sum I(ool) + P_o \sum I(hkl)}{\sum I(hkl) + P_o \sum I(hkl)} \qquad (4)$$

where I denotes the peak intensity of the current phase and P_0 =0.07 for Y-123.

3.2. Electrical Resistivity Measurements

The effect of partial substitution of Ba particles by Nd atoms on superconducting properties of the bulk Y-123 polycrystalline compounds is scrutinized by the temperature dependence of the electrical resistivity measurements in the temperature range of 10–300 K and the experimental observed results are graphically shown in Figure **2** and Figure **3**. Before a serious discussion, it should be noted here that both the transition temperatures and especially resistivity values belonging to the HcN superconductors are highly dependent on the concentration level of Nd inclusions inserted in the Y-123 crystal lattice. Furthermore, each sample presents a sharp transition to the superconducting state below the critical onset

temperature (T_c^{onset}) with the positive (dρ/dt) linear temperature dependence of resistivity as a result of the metallic conduct. This is related to the electron-phonon interaction in the crystal structure [31, 32] or logarithmic deviation in the state density at the Fermi level [33, 34]. Also, Figure **2** shows that the normal state resistivity of the superconducting Y-123 samples after T_c^{onset} value decreases monotonically with the increase in Nd content level up to y=0.100 in HcN, owing to both the increase of the metallic interaction between the superconducting grains and the optimization of the hole density and possible improvements in the lattice vibration [35]. Regarding the resistivity at room temperature (300 K), HcN4 samples reach the highest resistivity value (10.9 mΩ cm); conversely, the lowest resistivity value of 1,72 mΩ cm is attributed to the HcN3 samples. In other words, the magnitude of the room temperature resistivity changes by about a factor of 6 with the changes of the Nd inclusions in the HcN superconducting core. The main reason for the increase in the resistivity with the excessive Nd atoms is the decrease in mobile hole concentration (hole localization effect) of the Cu–sites in the Y-123 system, resulting in the phase transition from optimally doped to the underdoped position in the crystal array [36, 37]. Furthermore, the thermodynamic fluctuations or the opening of spin-gap mechanism (considered as the small curvatures above the (T_c^{onset}) values) confirm the penetration of the magnetic impurities (Nd nanoparticles) into the superconducting system [38]. This is a clue that the Cooper pairs exist even above the T_c values. In addition, the temperature dependent-electrical resistivity measurement results allow us to find the initial critical transition (T_c^{onset}) and offset critical transition (T_c^{onset}) temperatures. The numerical results of T_c^{onset} and T_c^{offset} can be encountered in Table **2**. Looking at the table, it is seen that all the Tc values

obtained rise with the increase of the Nd impurities in the HcN samples up to the value of y=0.100 beyond that they deteriorete fast owing to not only the lessening of the mobile hole concentration and average crystallite size but also the increase of the porosity and weak links between the grains [39]. When the doping level Nd is greater than y=0.100, there is a transition from optimally doped state to the underdoped state position of the HcN superconductors, which implies the decrease in the T_c^{offset} and T_c^{onset} values.

The maximum T_c^{offset} and T_c^{onset} values for the HcN3 sample are found to be approximately 94,84 K and 97,22 K, respectively, while the HcN4 compound has the minimum values of 60.72 K as (T_c^{offset}) and 84,92 K as (T_c^{onset}).

HcN5 samples exhibited in Figure **3** are semiconductor materials. All the ρ-T graphs of samples are demonstrated in the Figure **2** and Figure **3** below.

The long and short of it is that the optimum Nd concentration level in the crystal structure is recorded to be y=0.100 for the HcN superconducting phase formation as a result of the significantly improving the mobile hole concentration and interaction between the superconducting grains. It is also to be noted here that the variation of the values is considerably higher than that of the values as a result of the variation of the oxygen content level in the superconducting crystal structure by the partial replacement of Nd atoms on Ba-sites.
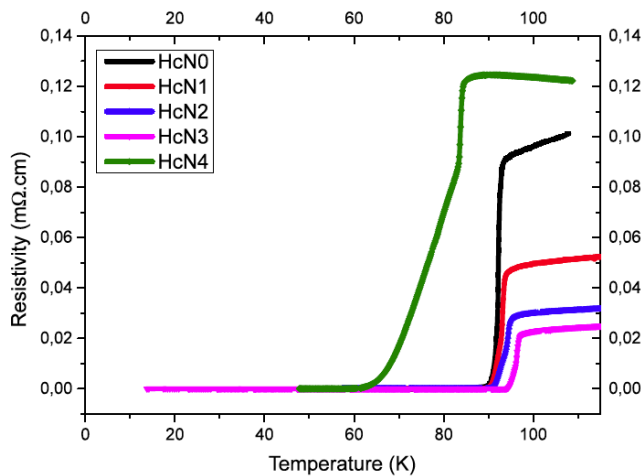
Figure 2: Temperature dependent-resistivity curves for the superconducting materials (HcN0-HcN4).

At the same time, the dramatic changes of the T_c^{offset} and T_c^{onset} values lead to the decrease/increase in

the degree of the broadening (ΔT_c). In this study, ΔT_c value is observed to decrease systematically from 4,75 K to 2,38 K with the increment of the Nd concentration level until y=0.100 after this critical value the value begins to increase steeply towards to 24,2 K for HcN owing to both the increased porosity, grain boundary resistivity and weak-links in the crystal structure [40] and the inhomogeneities (existence of CuO impurities) in the oxidation states of the superconducting grains [41].
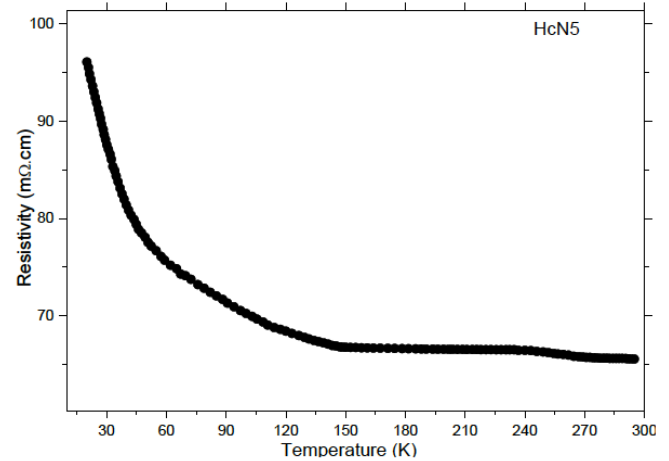
Figure 3: Temperature dependent-resistivity curves for the HcN5 samples.

3.3. Hole-Carrier Concentration Calculation

The hole-carrier concentrations per Cu ion, P, are calculated by the following equation [42]:

$$P = 0.16 - \left[\left(1 - \frac{T_c}{T_c^{max}} \right) / 82.6 \right]^{1/2} \tag{5}$$

where T_c^{max} is 92 K for Y-123 phase [43] and 85 K for Y-124 phase [44] and T_c values are read form Figure **2**.

When the compound is doped maximum, T_c is maximum at $P=P_0=0.16$. It is seen that the hole carrier concentration of the HcN3 samples reaching the highest critical temperature is higher than the others in Table **2**.

3.4. Transport Critical Current Density

Since the discovery of high-T_c superconductivity, many studies have been carried out to optimize the transport features of superconductors. The rare earth element (Re) doping or substitution is used to increase the critical current density J_c of $YBa_2Cu_3O_{7-\delta}$. Re-

Table 2:   **Experimental Values of Bulk Density, Porosity, DC Resistivity and Transport Critical Current Density for each Superconducting HcN Sample**

Samples	HcN Content	T_c^{onset}	T_c^{ofset}	ΔT_c	$\rho_{300\,K}$	J_c	Hole carrier	ρ (g/cm^3)	P (%)
	x	(K)	(K)	(K)	(mΩ cm)	(A cm$^{-2)}$	(n)		
HcN0	0.000	93.97	89.22	4.75	2.32	225	0.141	6.087	3.38
HcN1	0.025	94.22	89.97	4.25	2.25	237	0.143	6.133	2.65
HcN2	0.050	95.03	91.45	3.58	1.96	243	0.151	6.157	2.27
HcN3	0.100	97.22	94.84	2.38	1.72	251	0.140	6.214	1.37
HcN4	0.250	84.92	60.72	24.2	10.9	97	0.096	5.961	5.38
HcN5	0.500	…	…	…	…	…	…	…	…

doping causes crystal defects and improved vortex pinning [45].

In this part of the article, the critical current density (J_c) measurements allow us to investigate the effect of the Nd inclusions added to the Y-123 system on both the flux pinning mechanism and quality of the interaction between the grains in the crystal structure. Although, as it is known, J_c can be defined as the resistance against the applied temperature, current and magnetic field and the cuprate superconductors have an important handicap that their vortices move easily by reason of the grain misorientations [46]. In this work, we effort to improve the decay property of the Y-123 bulk superconductors by using highly dispersed Nd nanoparticles leading to the introduction of the nucleation centers (effective flux pinning centers) into the crystal structure. According to the experimental results obtained, it was determined that the self-field J_c values increase from 225 A.cm^{-2} (for the Ho constant sample) to 251 A.cm^{-2} (for the HcN3 compound) with the enrichment of the Nd particles in the HcN matrix up to a certain content value of y=0.100 beyond which it tends to decrease rapidly to 97 A.cm^{-2} at the constant temperature of 77 K. The systematic increase in the J_c values is related to tight bonding of the Nd nanoparticles to the nucleation centers [47]. The observed critical current density increase is due to Nd^{3+} ions occurring on the grain surface and normal cores of Abrikosov vortices [48]. In contrast, the significant decrease in the J_c value with the excess Nd atoms can be caused by the defects (worsening of the flux pinning centers) such as the pores, hole localization effect, voids, stacking defects, planar and micro defects (twin, domains, etc.) and weak links between the superconducting grains and grain boundary resistivity [49]. Another interesting result is that the J_c value is more sensitive to the Nd individuals in the HcN matrix than the T_c value.

An improvement in J_c is associated with not only the reduction of the porosity and poor bonding between the superconducting grains but also with the increase in the flux pinning centers, the average length of the cell parameter *c*, the grain size and their orientations [50]. Therefore, efforts have been made to develop effective pinning centers such as planar defects, stacking defects, and micro-defects with the help of methods such as operational procedure, variable preparation conditions including annealing ambient, chemical doping, substitution, transition metal evaporation, composition, heat treatment, additive type and amount [51, 52]. Furthermore, in the displacement process, the variation of some important superconductivity properties (critical current density, initial and offset critical temperatures, etc.) of the studied samples is related to the information obtained about both the position and charge of the doping metals. In other words, this technique is the most effective method for finding important clues about the mechanism of high temperature superconductivity [53, 54].

The critical current density in the crystals can be enhanced by adding effective flux pinning centers. As is well known, when a magnetic field applies to a type-II superconductor, it penetrates into the material in the form of vortices. Each vortex has a quantum flux $\Phi = h / 2e$ and consists of both a cylindrical core of a radius ξ (named as coherence length) and a current circulating around the core out to a distance λ (called as the penetration depth of the material) [55]. Therefore, the current flowing into the superconductor material creates energy dissipation as a result of the Lorentz force, causing the mobility of vortices and the loss of superconductivity in the material.

However, the mobility of the vortices can be minimized by introducing defects that fix these vortices. Therefore, the J_c value of a material is suitable for the flux pinning of vortices. In addition, effective flux pinning centers can be easily produced in a material because of the defects such as stacking faults, pores/voids, screw dislocations, twin boundaries, planar, and micro-defects [56-58].

3.5. SEM Analyses

The surface morphologies of Nd substituted bulk superconducting materials are depicted in the secondary electron image mode at 3000X and 5000X magnification by the scanning electron microscopy investigations. The resulting images are shown in Figure **4 a**-**c**.

Based on the figure, it can be easily said that the Nd foreigners added to the Y-123 system significantly changed the sample morphology. As the Nd individuals in Y-123 increase up to the critical value of y=0.100 in HcN, the microstructural properties regularly improve due to the presence of dense surface with fine coupling between grains.

Nevertheless, the surface morphology starts to deteriorate beyond the Nd concentration level of y=0.100 in HcN. In fact, it just gets worse and worse due to the presence of the porosity, partial melting, voids and cracks that cause new phase formations in the crystal structure. It should be noted here that we have already encountered the different minor phases (BaCuO$_2$, Y-247, and Y-124) for the HcN4 sample.

Furthermore, among the superconducting samples, the HcN3 sample achieves the smoothest and densest surface morphology, with the smoothest surface appearance, the largest crystalline (particle) size, the best texture, the lowest porosity, the best crystallinity, and the interaction between the superconducting grains. The long and short of it is that these samples except HcN5 exhibit all the essential features of the Y-123 phase in a good agreement with the Lotgering index data deduced from the XRD diffraction graphs.

3.6. The Bulk Density and Porosity Analyses

Now, Archimedes' water displacement method allows us to directly examine the variation of the grain boundaries transport properties in the Y-123 bulk superconducting materials. The calculated relative densities of the ceramics are subtracted from the density of the pure Y-123 system (approximately 6.357 g/cm^3) [23]. The calculated relative densities are given numerically in Table **2**. As can be seen from the table, it was observed that the density value in Nd inclusions in Ba sections increased from 6.087 g/cm^3 (for the HcN0 compound) to 6.214 g/cm^3 (for the HcN3 sample), increasing the Nd inclusions in the Y-123 system up to the certain value of y=0.100, beyond which the value is greatly reduced towards to 5.961 g/cm^3 (for the HcN5 material).
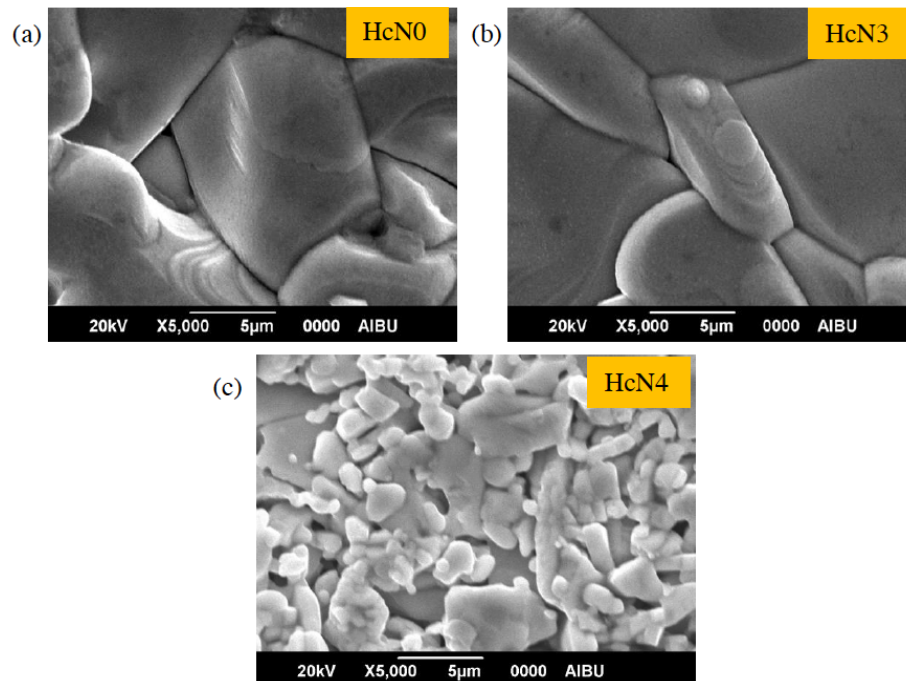
Figure 4: SEM micrographs for **a**) HcN0, **b**) HcN3, and **c**) HcN4 materials.

4. CONCLUSION

In the present study, we try to develop the mechanical, microstructural, electrical, and superconducting properties of the HcN superconducting ceramics by the partial replacement of Ba particles for Nd impurities in their crystal structures. The standard experimental measurements such as the bulk density, X-ray diffraction, dc resistivity, transport critical current density and scanning electron microscopy are made to obtain the optimum doping level of Nd. Furthermore, we have shown that the effect of hole (filling) localization effect, onset–offset critical transition temperature, spin-gap opening temperature, crystallinity, crystal plane alignments, crystal structure, grain size, phase purity, lattice parameters, and surface morphologies are critical in Ba-site Nd substituted Y-123 bulk superconductor. Each observed result from the experimental investigations proves that the important properties mentioned above are regularly improved by increasing the Nd content level at the Ba-sites in the superconducting core up to a critical value of y=0.100 (optimum), after which the properties tend to deteriorate significantly. Briefly, excessive (0.100 < y for only Nd in HcN) penetration of YBCO disrupts its crystal lattice.

The long and short of it is that the increase in the properties is the effect of reducing the porosity, grain boundary resistivity and weak-links in the crystal structure and improving the homogeneities in the oxidation states of the superconducting grains. It is attributed to the Nd element, which appears in the divalent and trivalent states in the crystal. In the former location state, the mechanical, electrical and especially superconducting properties of the Y-123 doped with Nd nanoparticles while the trivalent cation state significantly damages the properties due to the increased local structural distortions and the presence of mobile hole localization (filling) in the crystal system.

REFERENCES

[1] J. M. S. Skakle / Materials Science and Engineering R23 (1998) 1-40
https://doi.org/10.1016/S0927-796X(98)00010-2

[2] P. Karen, H. Fjel1vAg, A. Kjekshus, A. F. Andresen, J. Solid State Chern. 93 (1991) 163.
https://doi.org/10.1016/0022-4596(91)90285-P

[3] T. Leventouri, G. A. Soifer, M. Calamiotou, V. Perdikatsis, E. Lairokapis, J. Supercond. 8 (1995) 625.
https://doi.org/10.1007/BF00727448

[4] A. Pandey, R. Rajput, B. Sarkar, Y. S. Reddy, R. G. Sharma, Physica C 256 (1996) 335.
https://doi.org/10.1016/0921-4534(95)00677-X

[5] M. Ausloos, Ch. Laurent, H. W. Vanderschueren, A. Rulmont, P. Tarte, Solid State Commun. 68 (1988) 539.
https://doi.org/10.1016/0038-1098(88)90200-1

[6] N. K. Saritekin, M. Oz, C. Terzioglu, O. Gorur, G. Yildirim, Journal of Materials Science: Materials in Electronics 27 (2016) 6992-7003.
https://doi.org/10.1007/s10854-016-4655-6

[7] M. Öz, N. K. Saritekin, Ç. Bozkurt, G. Yildirim, Cryst. Res. Technol. 51, 380-392 (2016)
https://doi.org/10.1002/crat.201500337

[8] N. K. Sarıtekin, H. Bilge, M. F. Kahraman, Y. Zalaoğlu, M. Pakdil, M. Doğruer, G. Yıldırım, and M. Oz, 9th International Physics Conference of the Balkan Physical Union (BPU-9), AIP Conf. Proc. 1722, 140002 (2016)
https://doi.org/10.1063/1.4944192

[9] N. K. Sarıtekin, M. F. Kahraman, H. Bilge, Y. Zalao ğ lu, M. Pakdil, M. Doğruer, G. Yıldırım, and M. Oz, 9th International, Physics Conference of the Balkan Physical Union, AIP Conf. Proc. 1722, 140007 (2016).
https://doi.org/10.1063/1.4944197

[10] J. M. Tarascon, W. R McKinnon, L. H. Greene, G. W. Hull, E. M. Vogel, Phys. Rev. B 36 (1987) 226.
https://doi.org/10.1103/PhysRevB.36.226

[11] N. K. Sarıtekin, M. Dogruer, G. Yıldırım, C. Terzioglu, Journal of Materials Science: Materials in Electronics 25, 3127-3136 (2014)
https://doi.org/10.1007/s10854-014-1993-0

[12] N. K. Sarıtekin, M. Pakdil, G.Yıldırım, M. Öz, T. Turğay, Journal of Materials Science: Materials in Electronics 27, 956-965 (2016)
https://doi.org/10.1007/s10854-015-3839-9

[13] N. K. Sarıtekin, C. Terzioğlu, M. Pakdil, T. Turğay, G. Yıldırım, Journal of Materials Science: Materials in Electronics 27, 1854-1865 (2016)
https://doi.org/10.1007/s10854-015-3964-5

[14] F. Yong, Z. Lian, Z. Pingxiang, J. Ping, W. Xiaozu, L. Changxun and X. Mianrong, Journal of Superconductivity, Vol. 3 No. 2, (1992), 95-97.
https://doi.org/10.1007/BF00618051

[15] A. Hamrita, F. B. Azzouz, A. Madani and M. B. Salem, Physica C 472 (2012) 34-38.
https://doi.org/10.1016/j.physc.2011.10.003

[16] S. J. Hao, W. T. Jin, C. Q. Guo and H. Zhang, Physica C 475 (2012) 28-31.
https://doi.org/10.1016/j.physc.2012.01.013

[17] S. B. Guner, O. Gorur, S. Celik, M. Dogruer, G. Yildirim, A. Varilci and C. Terzioglu, J. Alloy. Compd. 540 (2012) 260-266.
https://doi.org/10.1016/j.jallcom.2012.06.082

[18] R. Shabna, P. M. Sarun, S. Vinu, A. Biju and U. Syamaprasad, Supercond. Sci. Technol. 22 (2009) 45016-45022.
https://doi.org/10.1088/0953-2048/22/4/045016

[19] S. Vinu, P. M. Sarun, R. Shabna, P. M. Aswathy, J.B. Anooja and U. Syamaprasad, Physica B 405 (2010) 4355-4359.
https://doi.org/10.1016/j.physb.2010.07.042

[20] N. K. Sarıtekin, M. Dogruer, Y. Zalaoglu, G. Yıldırım, C. Terzioglu, O. Gorur, Journal of Alloys and Compounds 659, 31-37 (2016)
https://doi.org/10.1016/j.jallcom.2015.10.295

[21] G. B. Akyuz, K. Kocabas, A. Yıldız, L. Ozyuzer and M. Ciftcioglu, J. Supercond. Nov. Magn. 24 (2011) 2189-2201.
https://doi.org/10.1007/s10948-011-1180-y

[22] M. A. Ansari, R. Nigam, V. P. S. Awana, A. Gupta, R. B. Saxena, H. Kishan, N. P. Lalla, V. Ganesan, A. V. Narlikar and C. A. Cardoso, J. Appl. Phys. 97 (2005) 10B104-1-10B104-3.
https://doi.org/10.1063/1.1850383

[23] O. Gorur, G. Yildirim, S. P. Altintas and C. Terzioglu, J. Mater. Sci: Mater. El. 24 (2013) 1842-1854.
https://doi.org/10.1007/s10854-012-1022-0

[24] M. H. Whangbo and C. C. Torardi, Science 249 (1990) 1143-1146.
https://doi.org/10.1126/science.249.4973.1143

[25] N. K. Sarıtekin, A. T. Üzümcü, Journal of Superconductivity and Novel Magnetism.
https://doi.org/10.1007/s10948-022-06209-5

[26] P. M. Sarun, S. Vinu, R. Shabna, A. Biju and U. Syamaprasad, J. Alloy. Compd. 472 (2009) 13-17.
https://doi.org/10.1016/j.jallcom.2008.04.103

[27] G. Yildirim, E. Yucel, S. Bal, M. Dogruer, A. Varilci, M. Akdogan, C. Terzioglu and Y. Zalaoglu, J. Supercond. Nov. Magn. 25 (2012) 231-237.
https://doi.org/10.1007/s10948-011-1284-4

[28] T. J. Kistenmacher, J. Appl. Phys. 64 (1988) 5067-5070.
https://doi.org/10.1063/1.342462

[29] A. Yildiz, K. Kocabas and G. B. Akyuz, J. Supercond. Nov. Magn. 25 (2012) 1459-1467.
https://doi.org/10.1007/s10948-012-1482-8

[30] W. Gao and J. B. Vander Sande, Supercond. Sci. Technol. 5 (1992) 318-326.
https://doi.org/10.1088/0953-2048/5/5/008

[31] S. Martin, M. Gurvitch, C. E. Rice, A. F. Hebard, P. L. Gammel, R. M. Fleming and A. T. Fiory, Phys. Rev. B 39 (1989) 9611-9613.
https://doi.org/10.1103/PhysRevB.39.9611

[32] N. K. Sarıtekin, Analytical Chemistry International 1, 67-82 (2021)
https://dx.doi.org/10.47204/ACI.1.2.2021.67-82

[33] D. M. Newns, P. C. Pattnaik and C. C. Tsuei, Phys. Rev. B 43 (1991) 3075-3084.
https://doi.org/10.1103/PhysRevB.43.3075

[34] K. Levin, J. H. Kim, J. P. Lu and Q. Si, Physica C 175 (1991) 449-522.
https://doi.org/10.1016/0921-4534(91)90258-Z

[35] M. B. Turkoz, S. Nezir, C. Terzioglu, A. Varilci and G. Yildirim, J. Mater. Sci: Mater. El. 24 (2013) 896-905.
https://doi.org/10.1007/s10854-012-0846-y

[36] O. Ozturk, E. Asikuzun, M. Erdem, G. Yildirim, O. Yildiz and C. Terzioglu, Mater. Sci: Mater. El. 23, (2012) 511-519.
https://doi.org/10.1007/s10854-011-0429-3

[37] Y. Zalaoglu, G. Yildirim, H. Buyukuslu, N. K. Saritekin, A. Varilci, C. Terzioglu, O. Gorur, Journal of Alloys and Compounds 631, 111-119 (2015)
https://doi.org/10.1016/j.jallcom.2015.01.095

[38] J. H. Koo and G. Cho, J. Phys. Condens. Matter 15 (2003) L729-L733.
https://doi.org/10.1088/0953-8984/15/46/L03

[39] O. Ozturk, E. Asikuzun and G. Yildirim, J. Mater. Sci: Mater. El. 24 (2013) 1274-1281.
https://doi.org/10.1007/s10854-012-0918-z

[40] A. Hamrita, F. B. Azzouz, A. Madani and M. B. Salem, Physica C 472 (2012) 34-38.
https://doi.org/10.1016/j.physc.2011.10.003

[41] N. K. Sarıtekin, Y. Zalaoglu, G. Yildirim, M. Dogruer, C. Terzioglu, A. Varilci and O. Gorur, J. Alloy. Compd. 610 (2014) 361-371.
https://doi.org/10.1016/j.jallcom.2014.04.037

[42] G. Yildirim, S. Bal and A. Varilci, J. Supercond. Nov. Magn. 25 (2012) 1655-1663.
https://doi.org/10.1007/s10948-012-1496-2

[43] T. Kucukomeroglu, E. Bacaksiz, C. Terzioglu and A. Varilci, Thin Solid Films 516 (2008) 2913-2916.
https://doi.org/10.1016/j.tsf.2007.05.075

[44] M. R. Persland, J. L. Tallon, R. G. Buckley, R. S. Liu, and N. E. Floer, Physica C 176, (1991). 95-105.
https://doi.org/10.1016/0921-4534(91)90700-9

[45] M. I. Petrov, Y. S. Gokhfeld, D. A. Balaev, S. I. Popkov, A. A. Dubrovskiy, D. M. Gokhfeld, K. A. Shaykhutdinov, Supercond. Sci. Technol. 21 085015 (2008).
https://doi.org/10.1088/0953-2048/21/8/085015

[46] G. Yildirim, Y. Zalaoglu, M. Akdogan, S. P. Altintas, A. Varilci and C. Terzioglu, J. Supercond. Nov. Magn. 24 (2011) 2153-2159.
https://doi.org/10.1007/s10948-011-1174-9

[47] E. H. Brandt, Rep. Prog. Phys. 58 (1995) 1465-1594.
https://doi.org/10.1088/0034-4885/58/11/003

[48] D. M. Gokhfelda, S. V. Semenova, D. A. Balaeva, I. S. Yakimov, A. A. Dubrovskiya, K. Y. Terentyeva, A. L. Freydmana, A. A. Krasikova, M. I. Petrova, Journal of Magnetism and Magnetic Materials 440 127-128 (2017).
https://doi.org/10.1016/j.jmmm.2016.12.089

[49] M. Dogruer, Y. Zalaoglu, G. Yildirim, A. Varilci and C. Terzioglu, J. Mater. Sci: Mater. El. 24 (2013) 2019-2026.
https://doi.org/10.1007/s10854-012-1051-8

[50] S. Bal, M. Dogruer, G. Yildirim, A. Varilci, C. Terzioglu, and Y. Zalaoglu, J. Supercond. Nov. Magn. 25, (2012) 847-856.
https://doi.org/10.1007/s10948-011-1360-9

[51] S. Jin, T. H. Tiefel, R. C. Sherwood, M. E. Davis, R. B. van Dover, G. W. Kammlott, R. A. Fasrnacht and H. D. Keith, Appl. Phys. Lett. 52 (1988) 2074-2076.
https://doi.org/10.1063/1.99751

[52] T. Egi, J. G. Wen, K. Koroda, H. Unoki and N. Koshizuka, Appl. Phys. Lett. 67 (1995) 2406-2408.
https://doi.org/10.1063/1.114562

[53] K. Fujita, T. Noda, K. M. Kojima, H. Eisaki and S. Uchida, Phys. Rev. Lett. 95, (2005) 097006-1-097006-4.

[54] K. Ozturk, S. Celik, U. Cevik and E. Yanmaz, J. Alloy. Compd. 433 (2007) 46-52.
https://doi.org/10.1016/j.jallcom.2006.06.082

[55] Y. Zalaoglu, G. Yildirim, and C. Terzioglu, J. Mater. Sci. Mater Electron 24 (2013) 239-247.
https://doi.org/10.1007/s10854-012-0723-8

[56] M. Tinkham, (1996) Introduction to Superconductivity, 2nd edn., (McGraw-Hill, New York).

[57] M. Pakdil, E. Bekiroğlu, M. Öz, N. K. Sarıtekin, G. Yıldırım, Journal of Alloys and Compounds 673, 205-214 (2016)
https://doi.org/10.1016/j.jallcom.2016.02.232

[58] N. K. Saritekin, M. Pakdil, E. Bekiroglu, G. Yildirim, Journal of Alloys and Compounds 688, 637-646 (2016)
https://doi.org/10.1016/j.jallcom.2016.07.203